Check for updates

A gradient screening approach for retired lithium-ion batteries based on X-ray computed tomography images†

Aihua Ran,‡[ab] Shuxiao Chen,‡[ab] Siwei Zhang,[ab] Siyang Liu,[ab] Zihao Zhou,[ab] Pengbo Nie,[ab] Kun Qian,[ab] Lu Fang,[ab] Shi-Xi Zhao,[b] Baohua Li,[b] Feiyu Kang,[ab] Xiang Zhou,[c] Hongbin Sun,[d] Xuan Zhang*[ab] and Guodan Wei [b] *[ab]

Accurate and efficient screening of retired lithium-ion batteries from electric vehicles is crucial to guarantee reliable secondary applications such as in energy storage, electric bicycles, and smart grids. However, conventional electrochemical screening methods typically involve a charge/discharge process and usually take hours to measure critical parameters such as capacity, resistance, and voltage. To address this issue of low efficiency for battery screening, scanned X-ray Computed Tomography (CT) cross-sectional images in combination with a computational image recognition algorithm have been employed to explore the gradient screening of these retired batteries. Based on the Structural Similarity Index Measure (SSIM) algorithm with 2000 CT images per battery, the calculated CT scores are closely correlated with their internal resistance and capacity, indicating the feasibility of CT scores to sort retired batteries. We find out that when the CT scores are larger than 0.65, there is high potential for a secondary application. Therefore, this pioneering and non-destructive CT score method can reflect the internal electrochemical properties of these retired batteries, which could potentially expedite the battery reuse industry for a sustainable energy future.

1. Introduction

Researchers have paid considerable attention to the degradation and ageing of lithium-ion batteries owing to their increasing demand in electric vehicles (EV), commercial aerospace, cell phones and laptops.[1] In addition, the revenues from the secondary application of retired lithium-ion batteries will indeed reduce the cost of battery production, which will, in turn, accelerate the development of energy storage and the EV industry.[2] However, the retired batteries usually need to be tested and sorted first so that suitable applications with lower requirements can be further explored to maximize the lifetime and safety of the battery.[3] In a recycling facility where tens of thousands of Li-ion cells need to be processed every day, sorting all the battery cells in an efficient way is one of the primary obstacles to be overcome in the retired battery market. In the meantime, the existing methods to sort out the retired batteries are inefficient, complicated and high cost since it typically involves with a charging and discharging process for several hours to complete.[4,5] Nowadays the systematic studies on the retired battery pack are very limited. Moreover, the capacity is heavily influenced by the depth of discharge,[6,7] the temperature,[8] the electrolyte[9] and usually several factors need to be taken into consideration together.[10,11] Therefore, it is in great need to explore a new and efficient sorting method to separate retired batteries into different levels for appropriately secondary applications such as in energy storage and electric motorcycles *et al.*

During the charging–discharging cycles for a battery, lithium ions move from the negative electrode to the positive electrode, which may lead to the battery expansion,[12] structural collapse,[13] lithium dendrite precipitation[14] and electrolyte decomposition to generate air bubbles.[15] These side reactions could cause damage to the battery internal structure, which is a potential indicator to represent the health or degradation of the batteries.

Generally, X-ray computed tomography (CT) is a powerful non-destructive examination technique that has applications in a variety of industrial and medical application, many previous studies have researched the structure of lithium ion battery, such as CT images can reflect the quality of newly produced lithium ion battery[16] and characterize the lithium movement with the help of Sn lithiation.[17] Also, X-ray CT is applied to

aTsinghua-Berkeley Shenzhen Institute (TBSI), Tsinghua University, Shenzhen, 518055, China. E-mail: weiguodan@sz.tsinghua.edu.cn; xuanzhang@sz.tsighua.edu.cn

bTsinghua Shenzhen International Graduate School, Tsinghua University, Shenzhen, 518055, China

cSchool of Data Science, Department of Mathematics, City University of Hong Kong, Tat Chee Avenue, Kowloon, Hong Kong SAR, China

dDepartment of Electrical Engineering, Tsinghua University, Beijing, China

† Electronic supplementary information (ESI) available. See DOI: 10.1039/d0ra03602a

‡ These two authors equally contributed to this work.

acquire high-spatial resolution three-dimensional (3D) images of materials and devices, allowing researchers to visually inspect and quantitatively analyze material structural properties due to its scan reconstructing capabilities.[18,19] X-ray CT images has previously been used to explore the microstructural properties of electrode materials in Li-ion batteries and has been shown to be an effective tool for diagnosing battery failure mechanisms post-mortem.[20,21] What's more, consecutive 3D images during *in situ* analyses can be used to quantify the microstructural evolution process, facilitating identification of potential failure and degradation mechanisms.[22] Due to the wide-spread of lab-based stand-alone CT systems, lots of researchers report that the CT can analyze the structure of the current collector,[23] the electrode structure,[24] the thermal runaway, gas production[25] and capacity.[26] Especially, CT images are useful for the examination of degraded cells,[27] structural deformations[28] can also facilitate post-mortem analysis by providing guidance for the mechanical degradation and indirect tracking of lithium diffusion in a commercial battery.[29] However, to date, this has all been conducted at the electrode-length scale, during normal operation, not used for quantitative detection of internal structural changes of the battery.[30]

Thus, this work aims to explore a non-destructive method to sort the retired batteries for secondary use. Because the CT images can visually show the structural defects on the cross-section images of the battery. A comprehensive analysis of the similarities of the cross sections of battery can obtain the CT score based on computational image recognition algorithm, which can reflect the state of health of the battery. We find that the CT scores are intrinsically correlated to the capacity and resistance of the batteries from a selection of retired cells. The electrochemical performance is closely related to the internal structure so that we can sort out the batteries retired from a battery pack based on the post-mortem analysis of CT images. Electrochemical test results have further validated the reliability of the CT score. In short, the correlation between CT score and electrochemical performance illustrate the power of computer image recognition algorithm assisted CT score to gradient screening of retired lithium-ion batteries.

2. Experiments

All the lithium ion batteries used in this work are from the dissembled pack of a motorcycle. Each cell is scanned in an industrial CT system (Werth TomoScope XS). Scanning resolution is between 10 to 20 micrometers. The X-ray tube is operated at 130 kV and 120 μA, corresponding to a spot size of 20 μm and the image intensifier is a 2D panel with 1024×144 elements. Distortion correction and computed tomography processing of the raw radiographs are performed using the BIR ACTIS 5 software package.

Sample preparation is accomplished by affixing them to a rotating platform. Each sample is affixed so that the longer axis of the object was parallel to the axis of rotation. For convention, we consider the axis of rotation the Z-axis and the perpendicular the X–Y plane. Each sample is positioned so that its radiograph, taken at its sample is point, fills approximately

80–90% of the image intensifier width. Since the image intensifier has 1024 elements of width, the in-plane (X–Y plane) resolution of an object is approximately given by: (widest dimension of the object)/(percentage of image intensifier utilized)/1024. For a new 18650 cell, that is approximately 18 mm in diameter, the typical in-plane resolution in this configuration would be approximately 22 μm. The samples are then rotated through platform, and a series of radiographs were collected by the ACTIS 5 software at each angle of rotation. This process is repeated at all necessary Z-height positions until each location throughout the height of the sample had been scanned which could be finished in one hour.

In total, each battery sample is imaged using 3000 views per full rotation. The ACTIS 5 software process the thousands of raw radiographs to reconstruct a series of two-dimensional "slices". A slice is a virtual cross-section of an object in an X–Y plane that represents a portion of the object's overall Z height; it is perpendicular to the axis of rotation. Each slice in the resulting data set is a gray scale 16 bit TIFF image file. In the case of the 18650 cell, the slice thickness was 30 μm, for a total of 2215 slices, and the resulting X–Y pixel dimensions were 22.46 μm for their cross-section images.

3. Results and discussions

In this work, we dismantled a retired battery pack used in an electric motorcycle to study the degradation of commercial lithium ion battery. Fig. 1 shows a schematic diagram of a typical 18650 lithium-ion battery with cylinder shape (18 mm in diameter and 65 mm in length), whereas the positive and negative electrodes are separated by a separator to prevent short circuit. The capacity of the pack is 8 A h and the voltage is 36 V and the pack is formed with 4 cells in parallel and 10 in series. Usually, retired batteries have internal structural defects that could affect their performance. However, these broken internal structures are not easily observed using conventional characterization methods.

Herein, we use CT technology to characterize the internal battery structures, as shown in Fig. 2, internal defects can be clearly expressed. From the longitudinal CT image shown in
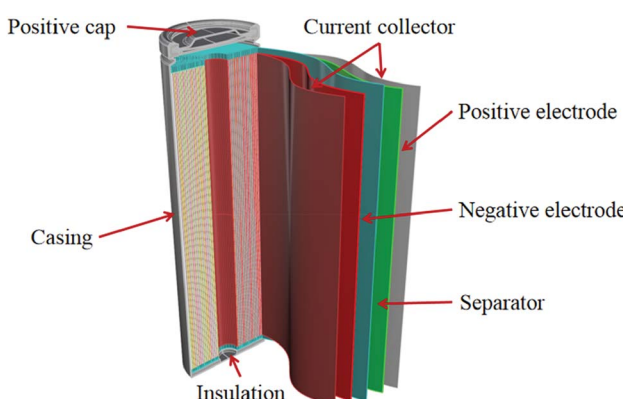

Fig. 1 Schematic diagram of a typical 18650 lithium ion battery.
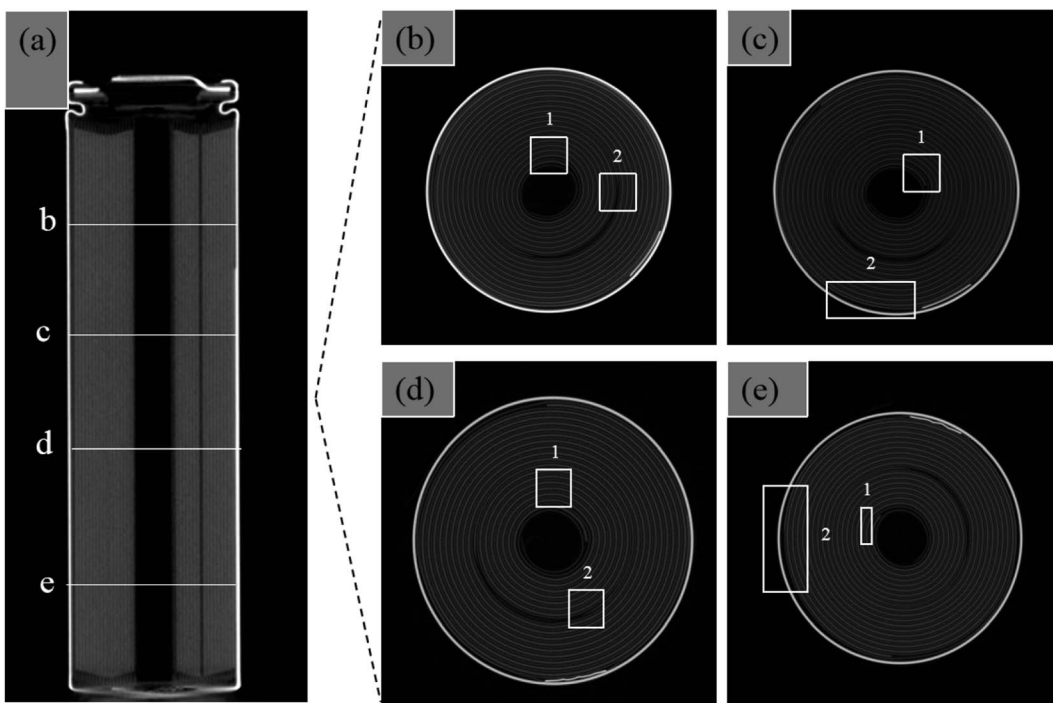
Fig. 2 CT images of retired lithium ion battery: longitudinal section (a) and different cross-sections (b–e). Position 1 and 2 are the weak parts in the battery internal structure.

Fig. 2(a), we can see whether the internal structure of the battery is deformed. From the perspective of safety, it can't be reused if the battery were deformed. Fig. 2(b)–(e) shows CT images from different cross-section locations labeled at b, c, d and e in one battery, we can clearly observe the layer-to-layer variation in position 1 in the center of the battery. The position 1, 2 is the position of the current collector, which belongs to the weak position in the battery, and there is obvious deformation. There are also many defects such as the shedding of the active material and the change between the electrode layers, which can't be directly seen by the naked eyes. These changes can cause damage to the battery and affect the battery life.

In this work, we perform electrochemical analysis on forty cells of the dismantled battery pack with 10 series group labeled from A to J (four batteries in each group). Fig. S1(a)† shows the open-circuit voltage (OCV) of the forty cells, there is little difference between each group. On the contrary, the resistance in Fig. S1(b),† the discharge capacity in Fig. S1(c)† and the capacity have a huge difference among the forty dismantled cells. The trend is the higher the resistance, the worse capacity, which means the failure of the cells. The capacity of four cells in one parallel is similar. The voltage is different in different series shown in Table S1.† And in Table S2,† it shows the distribution of the capacity. We sort the ten groups of cells with different electrochemical parameters shown in Table S1.† Capacity and internal resistance reflect aging of lithium ion battery better than the voltage. Cells in group C, D, G, H and J are close to zero. Table S2† shows most of the cells' capacity is less than 600 mA h. Only the capacity is above 1000 mA h, the battery could be chosen to further utilization. Therefore, the performance of

these 40 dismantled batteries is different. In order to better utilize the retired battery, effective sorting of retired batteries is particularly important.

To quantitatively characterize the state health of the retired battery, we firstly use CT score, calculated by the Structural Similarity Index Measure (SSIM) method with multiple CT images.[31] SSIM was initially designed to evaluate the structural similarity of original and distorted images to evaluate the quality of distorted images, here we apply this approach to evaluate the similarity of two images from different cross sections of a battery.

In the fundamental basis of using Structural Similarity Index Measure (SSIM) lies in the fact that the mathematical method of SSIM (Fig. 3), mining structural similarity information among images by constructing a formula through the mean value, variance and covariance, mainly does not require images being from an original image. In this method, the luminance and contrast related to the structure of battery are defined as the structure information in the image, which is based on the idea that pixels of each CT image have strong inter-dependencies especially when they are spatially close. Therefore, the key point is to calculate its similarity for the measured CT images.

The similarity measurement obtained by the SSIM measurement system can be composed of three comparison measurement between the samples of x and y: luminance (l), contrast (c), and structure (s) which will be defined as followed:

First, for discrete signals, we use the average grayscale as an estimate of the luminance measurement:
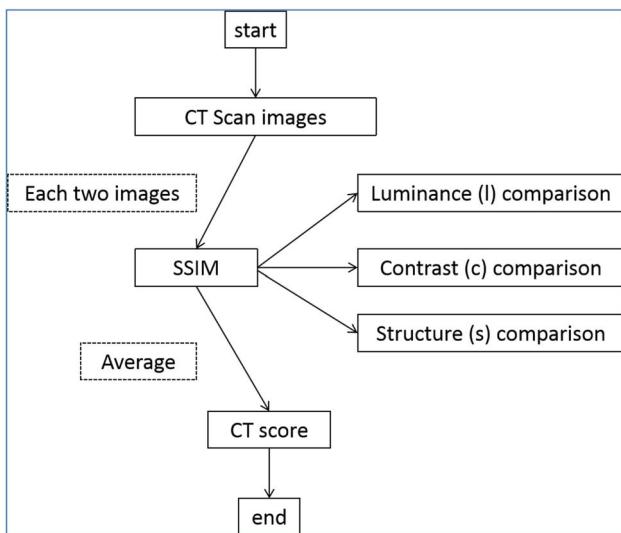
Fig. 3 CT score calculation flow chart. Each two CT images could get a CT score, the average of them are the output CT score of the tested battery.

$$\mu_x = \frac{1}{N} \sum_1^N x_i \tag{1}$$

Here x_i and y_i are two discrete non-negative signals that have been aligned with each other from two adjacent CT images of the tested battery (herein, these two image patches extracted from the same spatial location from two CT images being compared, respectively).

Therefore, the measurement system knows that the average gray value should be removed from the signal. For discrete signals $x - \mu_x$, the standard deviation can be used as the contrast estimate.

$$\sigma_x = \left(\frac{1}{N-1} \sum_{i=1}^N (x_i - \mu_x)^2 \right)^{\frac{1}{2}} \tag{2}$$

The contrast function $c(x,y)$ is a function of σ_x, σ_y.

Next, the signal is divided by its own standard deviation, and the structure contrast function is defined as a function of $\frac{(x - u_x)}{\sigma_x}$ and $\frac{(y - u_y)}{\sigma_y}$.

Finally, the three comparison modules are combined into a complete similarity measurement function:

$$S(x,y) = f(l(x,y), c(x,y), s(x,y)) \tag{3}$$

$S(x,y)$ should satisfy the following three conditions:
(1) Symmetry;
(2) Boundedness;
(3) Maximum uniqueness: $S(x,y) = 1$ if and only if $x = y$.
The brightness contrast function $l(x,y)$ is a function about μ_x, μ_y:

$$l(x,y) = \frac{2\mu_x\mu_y + C_1}{\mu_x^2 + \mu_y^2 + C_1} \tag{4}$$

The constant C_1 is to avoid system instability when $\mu_x^2 + \mu_y^2$ approaching zero.

In particular, we choose $C_1 = (K_1L)^2$, L is the number of gray levels of the image, for 8 bit grayscale images, $L = 255$, $K_1 \ll 1$. Eqn (4) satisfies the above three conditions.

Contrast function is defined by its own standard deviation:

$$c(x,y) = \frac{2\sigma_x\sigma_y + C_2}{\sigma_x^2 + \sigma_y^2 + C_2} \tag{5}$$

Constant $C_2 = (K_2L)^2$ and $K_2 \ll 1$. Eqn (5) still satisfies the above three conditions.

Structure comparison function:

$$S(x,y) = \frac{2\sigma_{xy} + C_3}{\sigma_{xy} + C_3} \tag{6}$$

Among them

$$\sigma_{xy} = \frac{1}{N-1} \sum_{i=1}^N (x_i - \mu_x)(y_i - \mu_y) \tag{7}$$

Finally, the three functions are combined to obtain the SSIM index function:

$$SSIM(x,y) = [l(x,y)]^\alpha [c(x,y)]^\beta [s(x,y)]^\gamma \tag{8}$$

Here $\alpha, \beta, \gamma > 0$, it is used to adjust the importance between the three modules.

To get the simplified form, let $\alpha = \beta = \gamma = 1, C_3 = \frac{C_2}{2}$, get:

$$SSIM(x,y) = \frac{(2\mu_x\mu_y + C_1)(2\sigma_{xy} + C_2)}{(\mu_x^2 + \mu_y^2 + C_1)(\sigma_x^2 + \sigma_y^2 + C_2)} \tag{9}$$

In this experiment, we tried $\alpha = \beta = \gamma = 1$. The CT score of good battery and bad battery is not very different, and the discrimination is relatively small. So these parameters are adjusted further. When $\alpha = 1$, $\beta = 7$ and $\gamma = 2$, CT score can better distinguish the batteries in this pack. In this work, we found $\alpha = 1$, $\beta = 7$ and $\gamma = 2$ are the most suitable and chosen to calculate the CT score. To note, for the values of α, β and γ in this test, it is difficult to find a universally applicable standard value. When it comes to distinguish a batch of batteries, several times needs to be tried to obtain a more ideal value which needs to be all positive numbers.

The CT score calculation flow chart is shown in Fig. 3. Firstly, we use former introduced industrial CT system to collect CT scan images of a retired battery. In this work, 2000 CT images are taken for each cell, that is, one taken every 100 times, and a total of 20 effective images could be obtained. Then the SSIM algorithm to compare the luminance (1), contrast (2) and structure (3) of each two images and get a score each time.

Hence, there are 190 $\left(C_{20}^2 = \dfrac{20 \times 19}{2} = 190\right)$ CT scores using formula (4) for a single battery and the CT score is the average of the 190 scores. It should be noted that in formula (4), due to the influence of luminance, contrast and structure are different, α, β and γ are parameters used to adjust the relative importance of the three components to the CT score. Among the three features, the contrast is the most important while the luminance is the least important.

Among the dismantled 40 cells, most of them have poor capacity without any value of reusing. Only the batteries from group B and group E have the capacity more than 50% of the initial capacity. So we select four used cells (named as B1, B2, E1, E3) to take their CT images and calculate the CT score shown in Fig. 4(a), and their electrochemical performance were measured to reflect the state of the retired batteries. The CT score of E1, E3, B1, and B2 are 0.566, 0.597, 0.752 and 0.854, respectively, suggesting that the health status of the battery increases in turn. The cycle performance of the resistance is tested to check the detail capability of these four cells at 1C rate on a battery testing system (LAND CT2001A, China) shown in Fig. 4(b)–(d). It shows B2 has the highest remaining capacity (Fig. 4(b)) and it is the most stable one (Fig. 4(c)). In contrast, E1 is the worst and most unstable. Correspondingly, the B2 has the minimum internal resistance with the charge–discharge cycling

numbers (Fig. 4(d)). The internal resistance of E1 increased with the cycling numbers sharply.

The incremental capacity is shown in Fig. 5(a), from B1, B2, E1 to E3, it can clearly see that the peak moving from left to right and disappearing in the bad cells, reflecting the loss of live lithium with the degradation of capacity. From Fig. 5(b) the open-circuit voltage (OCV) is closely connected with the state of charges (SOC). When the SOC is less than 30%, the OCV of the bad battery is higher than the better cells. When the SOC is more than 90%, the OCV of the better cells is higher than the bad ones.

It is obvious that the CT score is intrinsically correlated to the capacity, resistance and live lithium of the battery. However, as shown in Fig. 5(c), even if the capacity of the dismantled battery is close to that of the new battery, the CT score is only 90%, not 100%, because each cross-section of the new battery is also fundamentally different. When the CT score is 0.65–0.90, the capacity of the retired battery is about 95% of the new battery, and the capacity does not change much with the CT score. This type of battery has a great prospect of secondary utilization. When the CT score is 0.50–0.68, the battery capacity increases with the approximate CT score. This part of the battery also needs to test the internal resistance to determine further whether it can be used further. Comparing the CT score with the internal resistance in Fig. 5(d), the CT score of aged
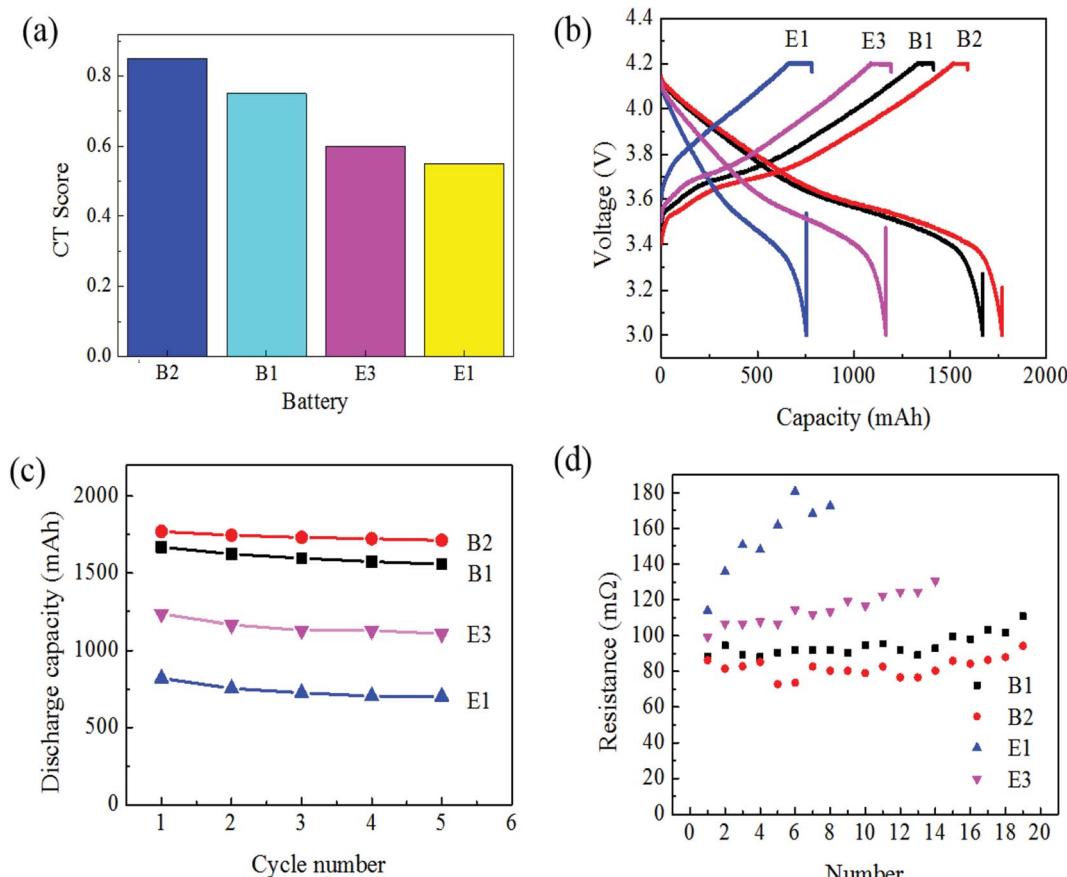

Fig. 4 CT score (a) and electrochemical performance of selected B1, B2, E1, E3: (b) discharge capacity; (c) cycle performance; (d) resistance.
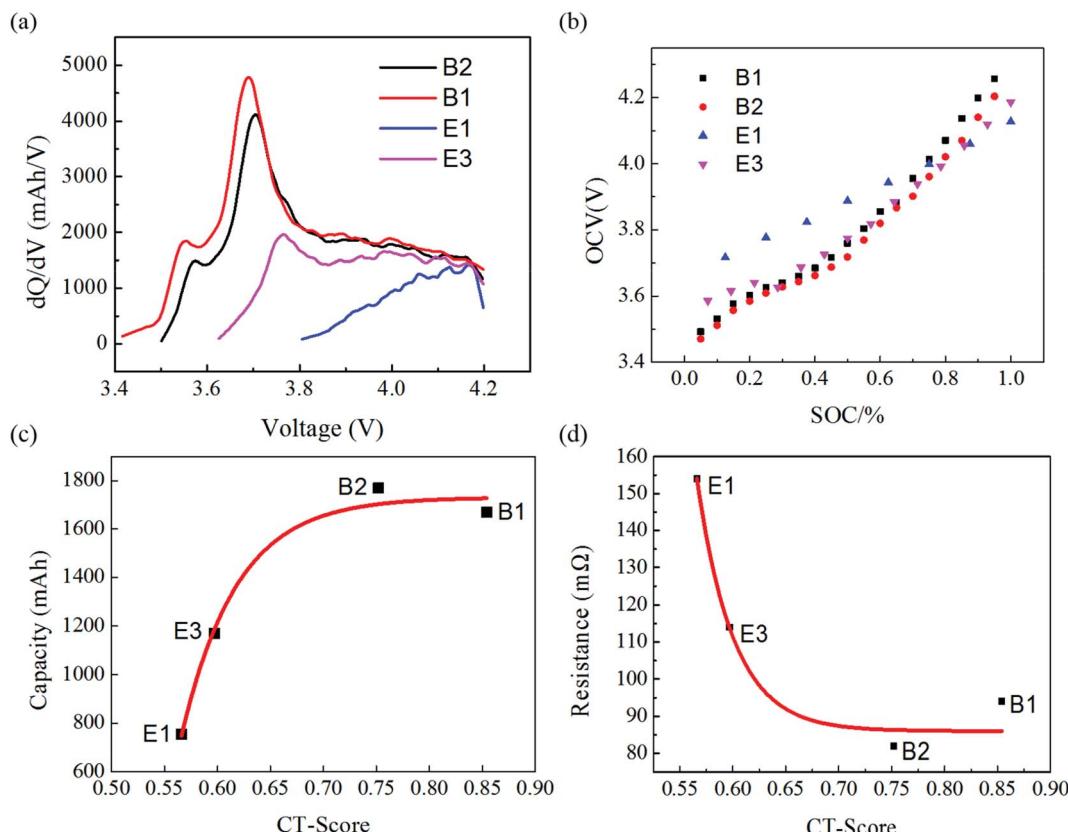
Fig. 5   The incremental capacity d*Q*/d*V* with voltage (a); the open-circuit voltage (OCV) with the state of charges (SOC) (b); the relationship between the CT scores and capacity (c); the relationship between the CT scores and resistance (d).

battery is less than 0.65 with a sharp change as well as its internal resistance is above 100 mΩ. For those battery with a CT score above 0.70, the internal resistance is below 85 mΩ. Obviously, the worse the battery performance, such as the lower the capacity, the greater the internal resistance, is indicating the more severe CT score attenuation and worse battery consistency. In other words, the more stable and higher CT score indicates the better battery performance and consistency. Therefore, the calculated CT score based on our proposed SSIM algorithm has been effectively reflected the state of health for the lithium batteries.

4.   Conclusions

In this study, the non destructive X-ray computed tomography (CT) technology is chosen to obtain the internal images of retired lithium ion battery. And CT images can clearly show the defects in battery structure caused by charging and discharging process, which is closely related to the state-of-life the battery. The CT score of lithium ion battery is calculated using SSIM method by analyzing the CT image, which can quantitatively reflect the state-of-life the battery, including its capacity, internal resistance, open circuit voltage. The data shows that when the CT score is lower than 0.55, the battery can be directly scrapped. Moreover, the battery with the CT score is higher than 0.68 shows higher capacity and smaller internal resistance,

suggesting it could be reused. Compared with the traditional electrochemical screening method, CT scan technology is non-destructive and quantitative, and can comprehensively reflect different electrochemical indexes.

Author contributions

Conceptualization and methodology, G. D. W., X. (Xuan) Z., X. (Xiang) Z., B. H. L., F. Y. K., H. B. S.; experiments and data analysis, A. H. R., S. X. C., K. Q., Z. H. Z., P. B. N., S. Y. L., S. W. Z.; discussion, G. W., L. F., S. X. Z. and F. K.; writing, A. H. R. and G. W.

Conflicts of interest

There are no conflicts to declare.

Acknowledgements

References

1 K. Lee, H. Jung, J. Chung, K. S. Kim, J. Song and J. Park, *Electrochim. Acta*, 2018, **281**, 274–281.

2 H. Gavln, S. Robert, K. Emma, R. Karl, G. Linda and A. Paul, *Nature*, 2019, **575**, 75–86.

3 R. R. Richardson, C. R. Birkl, M. A. Osborne and D. A. Howey, *IEEE Transactions on Industrial Informatics*, 2019, **15**, 127–138.

4 D. Kong, R. Wen, P. Ping, R. Peng, J. Zhang and G. Chen, *Int. J. Energy Res.*, 2018, **43**, 552–567.

5 R. Mingant, J. Bernard and V. Sauvant-Moynot, *Appl. Energy*, 2016, **183**, 390–398.

6 S.-h. Wu and P.-H. Lee, *J. Power Sources*, 2017, **349**, 27–36.

7 P.-H. Lee, S.-h. Wu, W. K. Pang and V. K. Peterson, *J. Power Sources*, 2018, **374**, 31–39.

8 R. Genieser, S. Ferrari, M. Loveridge, S. D. Beattie, R. Beanland, H. Amari, G. West and R. Bhagat, *J. Power Sources*, 2018, **373**, 172–183.

9 F. Horsthemke, A. Friesen, L. Ibing, S. Klein, M. Winter and S. Nowak, *Electrochim. Acta*, 2019, **295**, 401–409.

10 F. Camci, C. Ozkurt, O. Toker and V. Atamuradov, *J. Power Sources*, 2015, **278**, 668–674.

11 M. Naumann, M. Schimpe, P. Keil, H. C. Hesse and A. Jossen, *J. Energy Storage*, 2018, **17**, 153–169.

12 N. Nitta, F. Wu, J. T. Lee and G. Yushin, *Mater. Today*, 2015, **18**, 252–264.

13 B. Li, R. Shao, H. Yan, L. An, B. Zhang, H. Wei, J. Ma, D. Xia and X. Han, *Adv. Funct. Mater.*, 2016, **26**, 1330–1337.

14 F. Wu, S. Thieme, A. Ramanujapuram, E. Zhao, C. Weller, H. Althues, S. Kaskel, O. Borodin and G. Yushin, *Nano Energy*, 2017, **40**, 170–179.

15 Y. Zhong, M. Yang, X. Zhou and Z. Zhou, *Mater. Horiz.*, 2015, **2**, 553–566.

16 H. Chen and J. Shen, *PLoS One*, 2017, **12**, e0185922.

17 J. F. Gonzalez, D. A. Antartis, I. Chasiotis, S. J. Dillon and J. Lambros, *J. Power Sources*, 2018, **381**, 181–189.

18 F. Kong, R. C. Longo, C. Liang, D.-H. Yeon, Y. Zheng, J.-H. Park, S.-G. Doo and K. Cho, *Comput. Mater. Sci.*, 2017, **127**, 128–135.

19 J. Lamb and C. J. Orendorff, *J. Power Sources*, 2014, **247**, 189–196.

20 T. Kisters, E. Sahraei and T. Wierzbicki, *Int. J. Impact Eng.*, 2017, **108**, 205–216.

21 A. Pfrang, A. Kersys, A. Kriston, D. U. Sauer, C. Rahe, S. Käbitz and E. Figgemeier, *J. Power Sources*, 2018, **392**, 168–175.

22 O. O. Taiwo, J. M. Paz-García, S. A. Hall, T. M. M. Heenan, D. P. Finegan, R. Mokso, P. Villanueva-Pérez, A. Patera, D. J. L. Brett and P. R. Shearing, *J. Power Sources*, 2017, **342**, 904–912.

23 N. Aguiló-Aguayo, P. Amann, P. P. Espiñeira, J. Petrasch and T. Bechtold, *J. Power Sources*, 2016, **306**, 826–831.

24 I. Avdeev and M. Gilaki, *J. Power Sources*, 2014, **271**, 382–391.

25 D. P. Finegan, M. Scheel, J. B. Robinson, B. Tjaden, I. Hunt, T. J. Mason, J. Millichamp, M. Di Michiel, G. J. Offer, G. Hinds, D. J. L. Brett and P. R. Shearing, *Nat. Commun.*, 2015, **6**, 6924.

26 L. F. Li and J. W. Hou, *RSC Adv.*, 2018, **8**, 25325.

27 M. Y. Ali, W.-J. Lai and J. Pan, *J. Power Sources*, 2013, **242**, 325–340.

28 Y. Wu, S. Saxena, Y. J. Xing, Y. R. Wang, C. A. Li, W. K. C. Yung and M. Pecht, *Energies*, 2018, **11**, 925.

29 R. F. Ziesche, T. Arlt, D. P. Finegan, T. Heenan, A. Tengattini, D. Baum, N. Kardjilov, H. Markooter, In. Manke, W. Kockelmann, D. Brett and P. R. Shearing, *Nat. Commun.*, 2020, **11**, 777.

30 W.-J. Lai, M. Y. Ali and J. Pan, *J. Power Sources*, 2014, **248**, 789–808.

31 Z. Wang, A. C. Bovik, H. R. Sheikh and E. P. Simoncelli, *IEEE Trans. Image Process.*, 2004, **13**, 600–612.